Journal of Civil Structural Health Monitoring
https://doi.org/10.1007/s13349-024-00839-0

ORIGINAL PAPER

A two-step procedure for damage detection in beam structures with incomplete mode shapes

Martina Modesti[1] · Cristina Gentilini[2] · Antonio Palermo[1] · Edwin Reynders[3] · Geert Lombaert[3]

Received: 17 May 2024 / Accepted: 25 July 2024

Abstract
In this work, we present a two-step procedure for damage identification in beam structures exploiting modal curvature changes. The reconstruction of modal curvatures requires the knowledge of several mode shape components along the analyzed beam. This requirement is practically unachievable when mode shapes are identified via vibration-based monitoring using a limited number of accelerometers. To overcome this limitation, in the first step of the proposed procedure, we perform a mode shape expansion employing a reduced subset of measured modal components. The remaining measured components are used as control parameters to formulate a first hypothesis on damage location and extent. For this purpose, the expansion procedure is performed considering a number of possible damage scenarios, consisting of a location and a severity (loss of stiffness) of the damage. Using the Total modal assurance criterion (TMAC), we select the expanded modes with the highest degree of correspondence with the measured control components. These expanded modes are thus associated with a first guess of the damage location and severity. In the next step, this initial damage identification is verified through the computation of a modal curvature-based damage index. If the curvature-based damage identification confirms the previous identification, the damage location and extent are determined. The procedure can be easily extended to identify multiple simultaneously damaged elements. The approach is numerically validated using a benchmark beam modeled via finite elements, investigating the influence of different parameters such as noise, position of the control components and beam discretization on the identification success rate. Finally, the procedure is tested on two experimental specimens: a steel beam, with three different damage configurations and a concrete beam progressively damaged with multiple damage locations.

Keywords Damage identification · Beam structure · Flexibility matrix · Incomplete mode shape · TMAC · Concrete beam · Steel beam · Modal curvature

✉ Cristina Gentilini
cristina.gentilini@unibo.it

✉ Antonio Palermo
antonio.palermo6@unibo.it

Martina Modesti
martina.modesti2@unibo.it

Edwin Reynders
edwin.reynders@kuleuven.be

Geert Lombaert
geert.lombaert@kuleuven.be

[1] Department of Civil, Chemical, Environmental and Materials Engineering (DICAM), University of Bologna, Viale del Risorgimento 2, Bologna 40136, Italy

[2] Department of Architecture (DA), University of Bologna, Viale del Risorgimento 2, Bologna 40136, Italy

[3] Department of Civil Engineering, Belgium, KU Leuven, Kasteelpark Arenberg 40, Leuven 3001, Belgium

1 Introduction

Civil engineering structures are prone to damage during their lifetime. This risk is particularly significant in countries like Italy, where there is a large number of aged structures and infrastructures of public importance. Monitoring these structures is essential to early detect any damage and prevent potential local failures that could result in collapse and endanger human lives [1]. Indeed, recent bridge failures in Italy, such as the Morandi bridge in 2018 and the Massa Carrara bridge in 2020, have renewed the attention of the stakeholders and the scientific community on the importance of early detection of damages [2–6]. Regardless of the cause or mechanism—such as corrosion, chemical degradation, fatigue, or environmental influences—damage can alter the structure's dynamic response, leading, for instance, to a shift in natural frequencies

Published online: 09 August 2024

and changes in vibration modes. For this reason, many researchers and practitioners have focused on monitoring modal changes to detect, localize, and quantify damage in structures. Recent advances in vibration-based Structural Health Monitoring (SHM) methodologies of civil structures are summarized in a number of reviews, including Alvandi and Cremona [7], Doebling et al. [8], and more recently, Avci et al. [9]. In general, vibration-based identification methods can be roughly classified into three families: modal methods (e.g., [10, 11]), time-series methods (e.g., [12, 13]) and time-frequency methods (e.g., [14, 15]). Given the extensive nature of the topic under discussion, our focus is directed toward modal-based methods, which rely on the variation of modal parameters due to damage occurrence. Among these, methodologies based on changes in mode shapes and derived values, such as modal curvature, and flexibility matrix stand out. In particular, a commonly used technique for localizing damage in structures, which utilizes bending mode shapes, involves assessing the curvature difference between intact and damaged structures [16]. Since curvature is directly proportional to the inverse of bending stiffness, several methods have exploited this relationship to identify stiffness loss in structures [17]. The use of curvature changes offers an improvement over techniques that solely rely on modes of vibration, as it provides direct information into both the location and extent of damage. In [18, 19], a prediction of damage location and intensity in beam structures is obtained from measured modal displacement derivatives, preliminary smoothed to account for inaccuracies of mode shapes. Indeed, bending modes are used to derive the dynamic stiffness from modal curvature calculations. Other studies employ elastic curvature change as a damage indicator [20–22]. A damage factor based on curvature is presented in [11]. The damage index is calculated as the average of modal curvature variations across all measured mode shapes of the structure. Other methods to estimate curvature for damage identification purposes involve the pre-processing of the modal displacements before evaluating the curvature itself, for example, using the cubic spline interpolation, [10, 23]. Extension of identification methods based on curvature variations employ Frequency Response Function data instead of the computed modes of vibration, as presented in [24]. In [25], strain sensors as fiber-optic strain sensors are used for the direct operational identification of modal curvatures and subsequently for damage identification. Recently, in [26], as strain-based damage sensitive feature, the neutral axis position under bending deformation, which relates directly to the bending stiffness, is considered.

In the case of data acquisitions by means of accelerometers, a high spatial resolution of the modal components to calculate the modal curvature is required. This requirement can only be fulfilled by deploying a significant number of sensors, as highlighted in [27, 28].

To address this issue, this work proposes a procedure that reconciles the necessity to measure several modal components with the typically limited number of accelerometers available during on-site structure monitoring. In the literature, this gap has been addressed through dynamic expansion procedures, which enable the extraction of full-field dynamic responses of structures using measurements from discrete locations, as discussed in [29–31].

In this context, the expansion procedure is additionally employed to develop an initial hypothesis concerning the location and intensity of damage, which is then validated in the subsequent step. In the first step, we combine the modal expansion algorithm proposed in [32] with a grid-search procedure to generate a set of expansion operators associated with various damage scenarios, specifically, a damaged element with a given intensity of damage. The computation of the Total Modal Assurance Criterion (TMAC) enables us to select the set of damaged mode shapes and the corresponding damage scenario, forming an initial hypothesis regarding the location and extent of the damage.

In the second step, we evaluate the structure's flexibility matrix based on the assumed damage location and extent identified in the first step. From the flexibility matrix, we derive the Curvature Damage Index (**CDI**) to pinpoint the damaged beam element.

If the element indicated by the **CDI** index aligns with the one identified in the first step through the TMAC value, the damage location and extent are confirmed. If this verification fails, the algorithm iterates the procedure until the two-step check is validated. The procedure can be easily applied also to the case of multiple damaged scenarios as illustrated in the numerical examples and experimental tests. In particular, experimental data on a concrete beam, which were collected at KU Leuven (Belgium) [18, 19, 33, 34], are analyzed to identify a crack pattern extensively distributed along the beam span.

The remainder of the paper is organized as follows: Sect. 2 discusses the theoretical framework, introducing the curvature damage index based on the flexibility matrix. Section 3 focuses on the adopted procedure for modal expansion, while the two-step damage identification strategy is described in Sect. 4. In Sect. 5, the procedure is numerically validated on a statically undetermined beam, investigating the influence of several parameters on the performance of the method, such as noise, damage extent, beam discretization, as well as the position of measured modal components. In Sect. 6, the application of the method for damage localization and quantification on a steel beam and on a concrete beam tested in laboratory is described. Finally, Sect. 7 concludes the article by summarizing the key findings.

2 Theoretical framework

In this section, a procedure to determine the damage identification index by exploiting the lowest natural frequencies and mode shapes of the structure is illustrated. In particular, the modal curvatures of both healthy and damaged beams are evaluated using the flexibility matrix.

2.1 Flexibility matrix

Without loss of generality, we consider a linear elastic beam structure discretized into n_e elements for a total of n degrees of freedom. Modal characteristics, including circular frequencies and mode shapes, are obtained by solving the following eigenvalue problem:

$$(\mathbf{K} - \omega_i^2 \mathbf{M})\mathbf{U}_i = \mathbf{0} \quad \text{with} \quad i = 1, \dots, n \tag{1}$$

where $\mathbf{K}$ is the global stiffness matrix, $\mathbf{M}$ is the mass matrix, ω_i is the i-th circular frequency and $\mathbf{U}_i$ is the i-th mode shape. The i-th natural frequency of the structure f_i is defined as $f_i = \frac{\omega_i}{2\pi}$. Mass-normalized mode shapes $\mathbf{\Phi}_i$ are obtained as:

$$\mathbf{\Phi}_i = \frac{\mathbf{U}_i}{\sqrt{M_i}} \tag{2}$$

being M_i the $i-$th modal mass:

$$M_i = \mathbf{U}_i^{\mathrm{T}} \mathbf{M} \mathbf{U}_i \tag{3}$$

Mode shapes $\mathbf{\Phi}_i$, Eq. (2), are collected in the columns of the modal matrix $\mathbf{\Phi}$, whereas circular frequencies are collected in the diagonal spectral matrix $\mathbf{\Omega}^2$ as follows:

$$\mathbf{\Phi} = [\mathbf{\Phi}_1 \dots \mathbf{\Phi}_n] = \begin{bmatrix} \varphi_{11} & \dots & \varphi_{1n} \\ \vdots & \ddots & \vdots \\ \varphi_{n1} & \dots & \varphi_{nn} \end{bmatrix}, \quad \mathbf{\Omega}^2 = \begin{bmatrix} \omega_1^2 & \dots & 0 \\ \vdots & \ddots & \vdots \\ 0 & \dots & \omega_n^2 \end{bmatrix} \tag{4}$$

Mass normalization of the mode shapes leads to:

$$\mathbf{\Phi}^{\mathrm{T}} \mathbf{M} \mathbf{\Phi} = \mathbf{I} \tag{5}$$

$$\mathbf{\Phi}^{\mathrm{T}} \mathbf{K} \mathbf{\Phi} = \mathbf{\Omega}^2 \tag{6}$$

where $\mathbf{I}$ is the identity matrix. Since $\mathbf{\Omega}^2$ and $\mathbf{K}$ are positive definite, Eq. (6) can be inverted to obtain:

$$\mathbf{K}^{-1} = \mathbf{F} = \mathbf{\Phi}(\mathbf{\Omega}^2)^{-1}\mathbf{\Phi}^{\mathrm{T}} \tag{7}$$

where $\mathbf{F}$ is the flexibility matrix. Equation (7) can be rewritten as a summation considering all the n mode shapes and frequencies of the structure:

$$\mathbf{F} = \sum_{i=1}^{n} \frac{1}{\omega_i^2} \mathbf{\Phi}_i \mathbf{\Phi}_i^{\mathrm{T}} \tag{8}$$

Eventually, the same expression can be truncated to the first m modes:

$$\mathbf{F} \approx \sum_{i=1}^{m} \frac{1}{\omega_i^2} \mathbf{\Phi}_i \mathbf{\Phi}_i^{\mathrm{T}} \tag{9}$$

still obtaining an accurate prediction of the structure's flexibility, given the inverse proportionality between flexibility and circular frequencies [35]. In this regard, we remark that the computation of the flexibility matrix based on the lowest modal characteristics is particularly appealing in the context of structural health monitoring where only the lowest natural frequencies and mode shapes are generally estimated from sensor records [36].

2.2 Curvature damage index

Damage in a structural element, e.g., crack, corrosion, etc., leads to a reduction of the element cross section and, more in general to a loss of stiffness which, in turn, results in an increase of flexibility of the damaged element. This variation in flexibility can be used to detect and, eventually, locate the damage, as demonstrated in several examples presented in literature [36, 37]. To this purpose, we consider a structure in healthy conditions (superscript "H") and a structure in damaged conditions (superscript "D"), with circular frequencies ω_i^{H} and ω_i^{D}, and mode shapes $\mathbf{\Phi}_i^{\mathrm{H}}$ and $\mathbf{\Phi}_i^{\mathrm{D}}$, respectively.

Following Eq. (9), the related flexibility matrices are estimated from a reduced number m of mode shapes as:

$$\mathbf{F}^{\mathrm{H}} \approx \sum_{i=1}^{m} \frac{1}{(\omega_i^{\mathrm{H}})^2} \mathbf{\Phi}_i^{\mathrm{H}} (\mathbf{\Phi}_i^{\mathrm{H}})^{\mathrm{T}} \tag{10}$$

$$\mathbf{F}^{\mathrm{D}} \approx \sum_{i=1}^{m} \frac{1}{(\omega_i^{\mathrm{D}})^2} \mathbf{\Phi}_i^{\mathrm{D}} (\mathbf{\Phi}_i^{\mathrm{D}})^{\mathrm{T}} \tag{11}$$

Column $i-$th, $\mathbf{F}_i$, of the flexibility matrix corresponds to a displacement vector associated with a unit force applied to the i-th degree of freedom. From $\mathbf{F}_i$, it is possible to extract the 4×1 displacement vector $(\mathbf{u}_j)_i$, which collect the nodal displacements of the j-th element.

Considering the $j-$th element of the beam of length L_j and beam axis x in Fig. 1, the displacement vector $(\mathbf{u}_j)_i$, which collects the nodal displacements due to a unitary force applied to the i-th degree of freedom, is defined as:

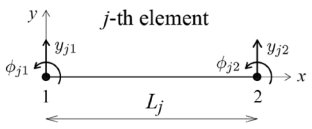

Fig. 1 j-th element of the beam structure

$$(\mathbf{u}_j)_i = \begin{bmatrix} y_{j1} & \phi_{j1} & y_{j2} & \phi_{j2} \end{bmatrix}_i^{\mathrm{T}} \tag{12}$$

where y_j is the vertical displacement, ϕ_j is the rotation, and subscripts "1" and "2" refer to the element nodes, respectively. Vector $(\mathbf{u}_j)_i$ for every element of the beam can be obtained from the $i-$th column of the flexibility matrix, as:

$$(\mathbf{u}_j)_i = \mathbf{T}_j \mathbf{F}_i \tag{13}$$

where $\mathbf{T}_j$ is a $4 \times n$ topological matrix. Transverse deflection $v_{ji}(x)$ and curvature $\chi_{ji}(x) = v''_{ji}(x)$ of the $j-$th element, are determined as:

$$v_{ji}(x) = \mathbf{N}(x)(\mathbf{u}_j)_i \tag{14}$$

$$\chi_{ji}(x) = \mathbf{B}(x)(\mathbf{u}_j)_i \tag{15}$$

where $\mathbf{N}(x)$ is the 1×4 matrix of the cubic shape functions and $\mathbf{B}(x)$ is the matrix of the second-order spatial derivatives of the shape functions.

Let us consider the displacements $(\mathbf{u}_j)_i^{\mathrm{H}}$ for the healthy structure and $(\mathbf{u}_j)_i^{\mathrm{D}}$ for the damaged one. The modal curvature change $\Delta\chi_{ji}$ of the $j-$th element can be computed as:

$$\Delta\chi_{ji}(x) = \mathbf{B}(x)\Delta\mathbf{u}_{ji} \tag{16}$$

where $\Delta\mathbf{u}_{ji}$ is:

$$\Delta\mathbf{u}_{ji} = (\mathbf{u}_j)_i^{\mathrm{D}} - (\mathbf{u}_j)_i^{\mathrm{H}} \tag{17}$$

Given the curvature change $\Delta\chi_{ji}$, Eq. (16), computed for each $j-$th beam element considering the i-th column of $\mathbf{F}$, the index G_{ji} is introduced as:

$$G_{ji} = \int_0^{L_j} \Delta\chi_{ji}^2(x)\mathrm{d}x = \Delta\mathbf{u}_{ji}^{\mathrm{T}} \left[\int_0^{L_j} \mathbf{B}(x)^{\mathrm{T}}\mathbf{B}(x)\mathrm{d}x \right] \Delta\mathbf{u}_{ji} \tag{18}$$

where G_{ji} is calculated for all n columns of matrix $\mathbf{F}$ and for all n_e beam elements and collected in matrix $\mathbf{G}$ (dimensions $n_e \times n$). The index G_{ji} is a measure of the change in the modal element strain energy normalized by the element bending stiffness.

Hence, for each row of matrix $\mathbf{G}$, its maximum value is computed and labeled as CDI_j:

$$CDI_j = \max_j \mathbf{G} \tag{19}$$

Each parameter CDI_j is collected in the Curvature Damage Index vector **CDI** (dimensions $n_e \times 1$), providing a damage indicator for each element (j) of the beam. The maximum value of **CDI** corresponds to the element with the highest variation in curvature compared to the healthy element and thus the most likely damaged one.

3 Modal expansion

The computation of the above mentioned index, Eq. (19), requires the full set of modal components to build the structure's flexibility matrix. Such components are usually computed from numerical models of the structure [35, 38]. Conversely, when the modal characteristics are directly estimated from experimental measurements, following, for example, standard Operation Modal Analysis approaches [39, 40], a limited number of sensors (e.g., accelerometers) is used to collect the records from the structures. As a result, a limited number of modal components can be estimated by processing these data. Moreover, for beam structures, obtaining direct estimates of nodal rotations is a challenging task.

In what follows, we adopt a modal expansion technique to exploit the availability of incomplete mode shapes for the estimation of flexibility matrices in healthy and damaged conditions, Eqs. (10) and (11). In particular, we employ the modal expansion technique originally illustrated in [32]. The fundamental steps of the modal expansion technique are here briefly illustrated. In the procedure, $\mathbf{K}$ and $\mathbf{M}$ are assumed to be positive definite and the eigenvectors $\mathbf{\Phi}_i$ are mass-normalized. First, we divide the structure's degrees of freedom n into two subsets: the known measured DOFs (master DOFs), labeled with k, and the unmeasured ones (slave DOFs), labeled with u, being $n = k + u$. For the sake of clarity, in the following the double subscript is used to indicate the dimension of the matrices.

The modal matrix of the structure, Eq. (4), can be partitioned in known ($\mathbf{\Phi}_{kn}$) and unknown ($\mathbf{\Phi}_{un}$) modal components as:

$$\mathbf{\Phi} = \begin{bmatrix} \mathbf{\Phi}_{kn} \\ \mathbf{\Phi}_{un} \end{bmatrix} \tag{20}$$

The known modal components $\mathbf{\Phi}_{kn}$ are expanded using a subspace iteration method [32] that allows to evaluate the unmeasured components $\mathbf{\Phi}_{un}$ through the expansion matrix $\mathbf{R}$, of dimensions $u \times k$:

$$\mathbf{\Phi}_{un} = \mathbf{R}\mathbf{\Phi}_{kn} \tag{21}$$

According to the method presented in [32], the matrix $\mathbf{R}$ is evaluated following an iterative scheme. The procedure is initialized by computing the expansion matrix $\mathbf{R}^{(0)}$ as:

$$\mathbf{R}^{(0)} = \mathbf{C}_{uk}\mathbf{C}_{kk}^{-1} \tag{22}$$

where $\mathbf{C}_{uk}$ and $\mathbf{C}_{kk}$ are the submatrices of matrix $\mathbf{C}$ defined as follows:

$$\mathbf{C} = \mathbf{K}^{-1}\mathbf{M}, \qquad \mathbf{C} = \begin{bmatrix} \mathbf{C}_{kk} & \mathbf{C}_{ku} \\ \mathbf{C}_{uk} & \mathbf{C}_{uu} \end{bmatrix} \tag{23}$$

At the generic i-th iteration, the $(i+1)$-th expansion matrix $\mathbf{R}^{(i+1)}$ can be calculated as:

$$\mathbf{R}^{(i+1)} = (\mathbf{C}_{uk} + \mathbf{C}_{uu}\mathbf{R}^{(i)})(\mathbf{C}_{kk} + \mathbf{C}_{ku}\mathbf{R}^{(i)})^{-1} \tag{24}$$

The iteration is performed until the following convergence criterion is satisfied:

$$\varepsilon = 1 - \frac{(\mathbf{r}_j^{(i+1)})^{\mathrm{T}}\mathbf{r}_j^{(i)}}{|\mathbf{r}_j^{(i+1)}||\mathbf{r}_j^{(i)}|} \leq q \qquad (j = 1, 2, ..., k) \tag{25}$$

with $\mathbf{r}_j^{(i)}$ and $\mathbf{r}_j^{(i+1)}$ being equal to the i-th and $(i+1)$-th approximations of the j-th column of the expansion matrix $\mathbf{R}$, respectively. In Eq. (25), symbol $|.|$ indicates the Euclidean norm and q is the maximum error imposed by the user. In [32], the proof of convergence is given and, for an infinite number of iterations, the convergence to the exact dynamic expansion operator is demonstrated.

4 Damage identification strategy

The modal expansion procedure discussed in the previous section requires the knowledge of the structural stiffness $\mathbf{K}$ and mass matrix $\mathbf{M}$ to compute matrix $\mathbf{C}$, Eq. (23), which is used to calculate the expansion operator $\mathbf{R}$, Eq. (21). For a structure in healthy conditions, for example soon after its construction, one can reasonably obtain an estimation of stiffness and mass matrices from calibrated finite element models. As a consequence, the full eigenvectors and circular frequencies are obtained from Eq. (1) and the flexibility matrix $\mathbf{F}^{\mathrm{H}}$ is readily available and the expansion procedure is not needed. Nonetheless, finite element models can be affected by modeling errors and, in structural health monitoring approaches, it is current practice to consider incomplete experimental mode shapes, which more accurately represent the response of the actual system, [39, 41, 42]. Following this approach, we consider a network of sensors on the structure (k monitored DOFs) from which an incomplete set of m mode shapes, $\mathbf{\Phi}_{km}^{\mathrm{H}}$ is estimated. The monitored (known) modal components $\mathbf{\Phi}_{km}^{\mathrm{H}}$ can be expanded to obtain the complete modal matrix $\mathbf{\Phi}^{\mathrm{H}}$:

$$\mathbf{\Phi}^{\mathrm{H}} = \begin{bmatrix} \mathbf{\Phi}_{km}^{\mathrm{H}} \\ \hline \mathbf{\Phi}_{um}^{\mathrm{H}} \end{bmatrix} \tag{26}$$

where the unknown $\mathbf{\Phi}_{um}^{\mathrm{H}}$ components are computed from Eq. (21):

$$\mathbf{\Phi}_{um}^{\mathrm{H}} = \mathbf{R}^{\mathrm{H}}\mathbf{\Phi}_{km}^{\mathrm{H}} \tag{27}$$

being $\mathbf{R}^{\mathrm{H}}$ the expansion matrix of the healthy structure. It should be noted that $\mathbf{R}^{\mathrm{H}}$ is calculated from the stiffness and mass matrices obtained from the numerical model. Nonetheless, in the present procedure, the use of the FE model is limited to the calculation of the operator $\mathbf{R}^{\mathrm{H}}$, since in the expansion procedure the experimentally determined modal components are used to obtain a more reliable estimate of the complete mode shapes.

Conversely, when a damaged structure is monitored, the stiffness matrix $\mathbf{K}^{\mathrm{D}}$ is not a priori known. Indeed, the definition of the damaged stiffness matrix is the object of the monitoring procedure and requires the identification, localization and quantification of the damage.

In our approach, we suppose that damage does not influence the mass matrix $\mathbf{M}$ of the structure. Hence, the definition of the expansion operator $\mathbf{R}^{\mathrm{D}}$ depends only on the stiffness matrix $\mathbf{K}^{\mathrm{D}}$.

In what follows, we propose to evaluate the expansion operator $\mathbf{R}^{\mathrm{D}}$ adopting a grid-search procedure, where the stiffness matrix $\mathbf{K}^{\mathrm{D}}$ is computed by changing location and intensity of damage in the elements of the FEM structure. A first estimate of the damage location and extent is then obtained using a Modal Assurance Criterion-based approach.

In the second step of the identification procedure, the correctness of this first hypothesis is verified through the evaluation of the **CDI** vector, Eq. (19). The two-step procedure is illustrated in detail in the following.

4.1 First step identification procedure: selection of the expansion operator for the damaged structure

In the first step of the identification procedure, we arrange the monitored (known) k components of the lowest m mode shapes of a damaged structure in two subsets: a subset of b of modal components, collected in the matrix $\mathbf{\Phi}_{bm}^{\mathrm{D}}$, with $b < k$, to be used as the base for the modal expansion, and the remaining known components, collected in the matrix $\mathbf{\Phi}_{cm}^{\mathrm{D}}$, with $c = k - b$, used as control components. The key point of the proposed approach is to exploit the subset c of measured components to verify the accuracy of the expanded modes.

As a result, the $n \times m$ modal matrix of the damaged structure $\mathbf{\Phi}^{\mathrm{D}}$ is partitioned as:

$$\mathbf{\Phi}^{\mathrm{D}} = \begin{bmatrix} \mathbf{\Phi}_{km}^{\mathrm{D}} \\ \hline \mathbf{\Phi}_{um}^{\mathrm{D}} \end{bmatrix} = \begin{bmatrix} \mathbf{\Phi}_{bm}^{\mathrm{D}} \\ \mathbf{\Phi}_{cm}^{\mathrm{D}} \\ \hline \mathbf{\Phi}_{um}^{\mathrm{D}} \end{bmatrix} \tag{28}$$

being $\mathbf{\Phi}_{um}^{\mathrm{D}}$ the unknown mode shape components. At this stage, a grid-search procedure is performed considering $j = 1, \ldots, e \times d = n_{tot}$ damage scenarios obtained by locating the damage in e different elements with d different damage

intensities. Hence, each damage scenario comprises a single damaged element with a given damage intensity.

Note that, in this phase, only the components $\mathbf{\Phi}^{\mathrm{D}}_{bm}$ of Eq. (28) are expanded, following Eqs. (21)–(24). In particular, we consider j different expansion matrices $(\mathbf{R}^{\mathrm{D}}_{rb})_j$, with $r = c + u$, obtained from the corresponding damaged stiffness matrices $\mathbf{K}^{\mathrm{D}}_j$. A dataset of j expanded mode components $(\mathbf{\Phi}^{\mathrm{D}}_{rm})_j$, with dimensions $r \times m$, is thus obtained as:

$$(\mathbf{\Phi}^{\mathrm{D}}_{rm})_j = (\mathbf{R}^{\mathrm{D}}_{rb})_j \mathbf{\Phi}^{\mathrm{D}}_{bm} \tag{29}$$

We remark that each set of expanded mode shapes contains the control components $(\mathbf{\Phi}^{\mathrm{D}}_{cm})_j$ as:

$$(\mathbf{\Phi}^{\mathrm{D}}_{rm})_j = \begin{bmatrix} \mathbf{\Phi}^{\mathrm{D}}_{cm} \\ \mathbf{\Phi}^{\mathrm{D}}_{um} \end{bmatrix}_j \tag{30}$$

which are herein used to select the correct expansion operator $(\mathbf{R}^{\mathrm{D}}_{rb})_j$. In particular, we measure the degree of correspondence between each set of expanded control components $(\mathbf{\Phi}^{\mathrm{D}}_{cm})_j$ and the measured ones $\mathbf{\Phi}^{\mathrm{D}}_{cm}$. To this purpose, we exploit the Total Modal Assurance Criterion TMAC [35], defined as the product of the MAC between the first m modes of vibration:

$$\mathrm{TMAC} = \Pi_{i=1}^{m} \mathrm{MAC}(\mathbf{\Phi}^{\mathrm{D}}_{cm}, (\mathbf{\Phi}^{\mathrm{D}}_{cm})_j) \tag{31}$$

The largest TMAC value identifies the damage scenario $\bar{D} = (\bar{e}, \bar{d})$ and the related damaged stiffness matrix $\mathbf{K}^{\bar{\mathrm{D}}} = \mathbf{K}^{\mathrm{D}}(\bar{e}, \bar{d})$. Hence, a first estimate of damage, in terms of damage position in the element $\bar{e}$ with damage intensity $\bar{d}$, is obtained. The accuracy of this identification is then verified in the second step of the procedure by computing the damage identification index, as illustrated in the following.

We point out that the division of the known modal components is a key element of the identification first step, since it allows to formulate a hypothesis on the damage location and severity using information extracted from experimental results (e.g., the control components). The number of control components should be selected to calculate the TMAC value in Eq. (31) (e.g., $c >= 3$).

4.2 Second step identification procedure: CDI step

From the knowledge of the damaged stiffness matrix $\mathbf{K}^{\bar{\mathrm{D}}}$, we compute the expansion operator $\mathbf{R}^{\bar{\mathrm{D}}}_{uk}$ to obtain the unknown components $\mathbf{\Phi}^{\bar{\mathrm{D}}}_{um}$ from the full set of measured modal components $\mathbf{\Phi}^{\mathrm{D}}_{km}$:

$$\mathbf{\Phi}^{\bar{\mathrm{D}}}_{um} = \mathbf{R}^{\bar{\mathrm{D}}}_{uk} \mathbf{\Phi}^{\mathrm{D}}_{km} \tag{32}$$

As a result, the $n \times m$ modal matrix of the damaged structure $\mathbf{\Phi}^{\bar{\mathrm{D}}}$ is estimated as:

$$\mathbf{\Phi}^{\bar{\mathrm{D}}} = \begin{bmatrix} \mathbf{\Phi}^{\mathrm{D}}_{km} \\ \mathbf{\Phi}^{\bar{\mathrm{D}}}_{um} \end{bmatrix} \tag{33}$$

Given the complete mode shapes $\mathbf{\Phi}^{\bar{\mathrm{D}}}$ and circular frequencies ω^{D}_i (supposed to be known from experimental measures), the flexibility matrix $\mathbf{F}^{\bar{\mathrm{D}}}$, Eq. (11), is evaluated and the Curvature Damage Index (**CDI**) vector is determined, Eq. (19). The damaged element, namely e^{CDI}, is identified as the one with the highest value of **CDI**. The identification procedure of damage successfully terminates if the damaged element e^{CDI} corresponds to the $\bar{e}$ element identified by the TMAC-based selection and, correspondingly, the damage extent $\bar{d}$ is also determined. If not, the second step of the identification procedure is carried out again, by selecting the element and damage intensity indicated by the second largest TMAC value. The two elements e^{CDI} and $\bar{e}$ may not coincide due to uncertainties and noise.

Once a first damaged element and the related damage intensity are determined, the same algorithm can be used to search for possible additional damages. The second identification cycle starts from the grid-search step that is repeated $(e-1) \times d + 1$ times, accounting for the first damaged element with location and severity identified in the first step. Note that the scenario in which only one element is damaged (second element with zero damage) is taken into account in the procedure.

It is worth to emphasize that the second step of the procedure is fundamental to ensure the accuracy of the method, as the real damaged element may not necessarily yield the highest TMAC value due to noise and uncertainties. Additionally, TMAC values reflect only changes in mode shapes, while the CDI step includes both frequency and mode shape information through the flexibility matrix. Hence, the damage element selected in the first step is detected as the real damage location only when it is also indicated by the second one (CDI step).

5 Numerical simulations

The performance of the two-step algorithm is tested starting from the study of a statically indeterminate beam structure, [34]. Damage is modeled as a reduction of the element Young's modulus. Single damage scenarios, considering several levels of damage severity (reduction is stiffness) as well as noise are considered. Double damage scenarios are investigated as well.

5.1 Single damage scenarios

The structure under analysis is represented in Fig. 2. For the damage identification procedure, we monitor all the degrees

of freedom in the vertical direction ($k = 22$ measured DOFs), while rotations are unknown ($u = 25$ unknown DOFs). Among the measured DOFs, we choose 5 components as control DOFs ($c = 5$) and the remaining 17 DOFs are taken as the base for expansion ($b = 17$). As control components, the vertical displacements at nodes 5, 7, 15, 17, and 21 are selected in order to have a fairly even distribution along the beam. In all the simulations, four mode shapes ($m = 4$) are employed to approximate the flexibility matrix [5, 6].

The elastic modulus is reduced by 30% for one element in turn ($d = 30\%$). A noise level $p = 3\%$ is applied to the mode shape components, a value which is deemed reasonable to include both sensor noise and environmental variability. In particular, the $\varphi_{ij}^{\mathrm{D}}$ component of the i-th mode shape at the j-th degree of freedom of the damaged structure is computed as the mean of 100 $\hat{\varphi}_{ij}^{\mathrm{D}}$ mode components polluted according to:

$$\hat{\varphi}_{ij}^{\mathrm{D}} = \varphi_{ij}^{\mathrm{D}}(1 + p \cdot \delta) \tag{34}$$

with δ being a random instance of a uniform distribution between -1 and 1, and p representing the noise percentage. In the numerical simulations, mode shapes are obtained from Eq. (1).

Fig. 3 shows the identification results obtained in absence of noise. Notably, identifications are always successful (identification equal to 1). For a noise level $p = 3\%$, the rate of successful identifications, namely the number of correct identifications over 100 runs, is represented in the histograms of Fig. 4. The identification is deemed correct when the damaged element is properly identified in both the two identification steps. Quantification of damage is not considered at this stage. All elements demonstrate a damage detection success rate of over 60%, except for elements 1 and 24 adjacent to the supports. This may be attributed to the reduced sensitivity to curvature changes experienced closed to the support regions.

To investigate the possible influence of the beam discretization on the previous results, the beam is divided in 12

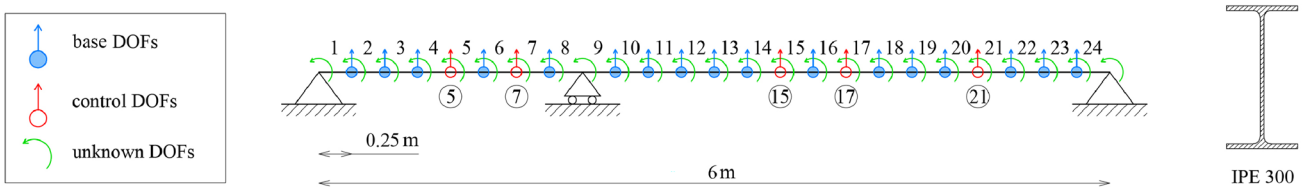

Fig. 2 Schematic of the beam: FE discretization (24 elements), DOFs classification and beam cross-section

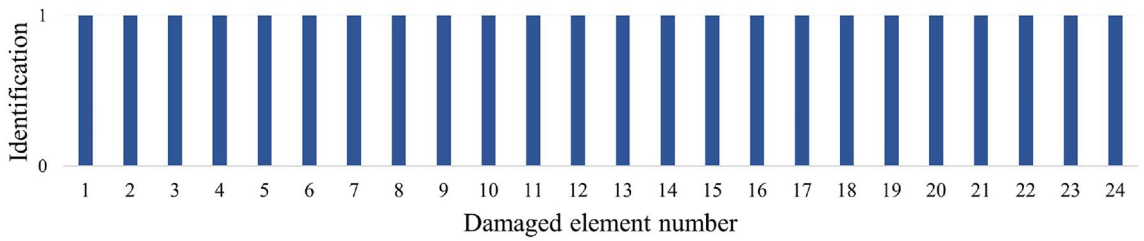

Fig. 3 Number of correct identifications (0 or 1) in single damage scenarios (damage extent $d = 30\%$) with noise $p = 0\%$

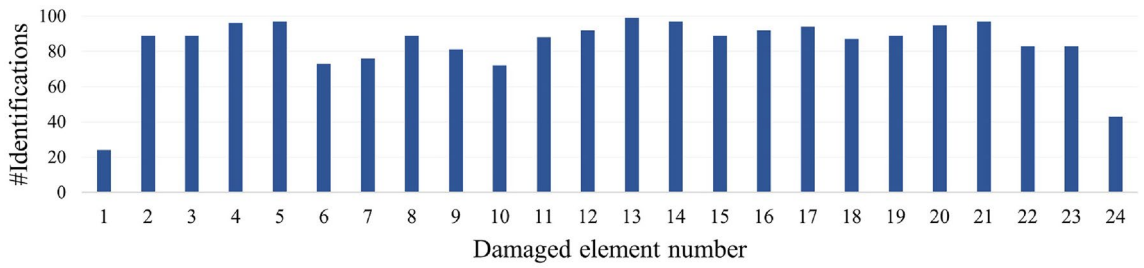

Fig. 4 Number of correct identifications over 100 runs in single damage scenarios (damage extent $d = 30\%$) with noise $p = 3\%$, considering the beam discretized in 24 elements

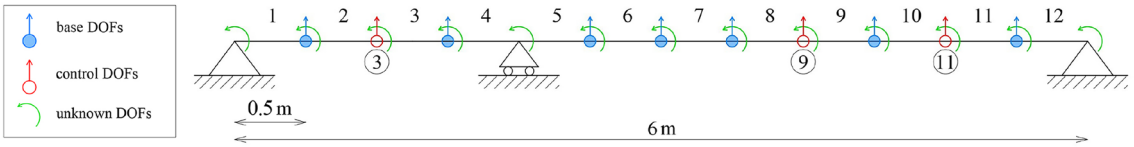

Fig. 5 Schematic of the beam: FE discretization (12 elements) and DOFs classification

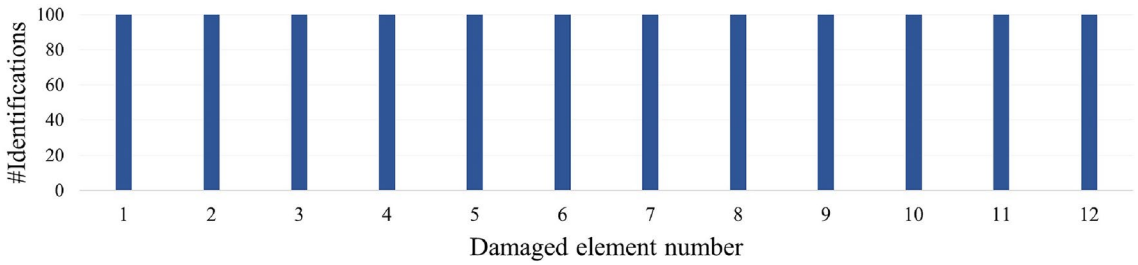

Fig. 6 Number of correct identifications over 100 runs in single damage scenarios (damage extent $d = 30\%$) with noise $p = 3\%$, considering the beam discretized in 12 elements

Table 1 Random configurations of control DOFs

Configuration	Control DOFs
C1	3, 9, 11
C2	4, 7, 12
C3	2, 11, 12
C4	2, 7, 10
C5	3, 8, 10
C6	2, 6, 9
C7	3, 6, 7
C8	2, 6, 11
C9	4, 8, 9
C10	4, 6, 10

elements, see Fig. 5. The following parameters are assumed in the calculations: all the vertical DOFs are supposed to be measured ($k = 10$), rotations are unknown ($u = 13$), while vertical displacements at nodes 3, 9 and 11 are used as control components ($c = 3$). An elastic modulus reduction $d = 30\%$ and a noise level $p = 3\%$ are considered.

We observe from Fig. 6 that all identifications are successful, even those related to elements close to the external constraints. This suggests that a coarser discretization of the structure leads to improved identification results because damage affects a longer element compared to a finer mesh.

To investigate the influence of the control DOFs position on the identification results, ten different random configurations are tested on the 12-element beam, keeping the number of control DOFs equal to 3. Specifically, each configuration is randomly generated considering one control DOF between nodes 2 and 4 (located to the left of the central support) and two control DOFs positioned between nodes 6 and 11 (between the central and the right support). The studied configurations are summarized in Table 1.

For the sake of brevity, results related only to three different configurations are reported in the following.

The studied damage scenarios consider an elastic modulus reduction $d = 10\%$ for each element in turn, with a noise level $p = 3\%$.

In Figs. 7a), 7b), and 7c), the success rates of damage identification using configurations C3, C4, and C6 are depicted, respectively. It is observed that for C4 and C6, the number of correct identifications is similar, with a success rate exceeding 80%. Conversely, configuration C3, Fig. 7a), shows a lower success rate, especially for the first seven elements (with a correct identification rate around 60%). This decrease can be attributed to the presence of two control sensors positioned next to each other (at positions 11 and 12), which are located near the lateral beam support.

The comparison between all the ten control configurations is summarized in Fig. 7, where the average number of identified elements vs. damage extent is reported. As expected, the average of successful identifications increases with the level of damage intensity (from 5% to 30%). Additionally, we observe that the identification trend for all the different control configurations is similar, except for C3 and C7 configurations (dashed lines). As mentioned earlier, these two configurations are characterized by two control nodes positioned closely to each other and near a support (Fig. 8).

In conclusion, except for some configurations where control DOFs are situated near each other and to the supports, the success rate is not very sensitive to the position of control DOFs along the structure.

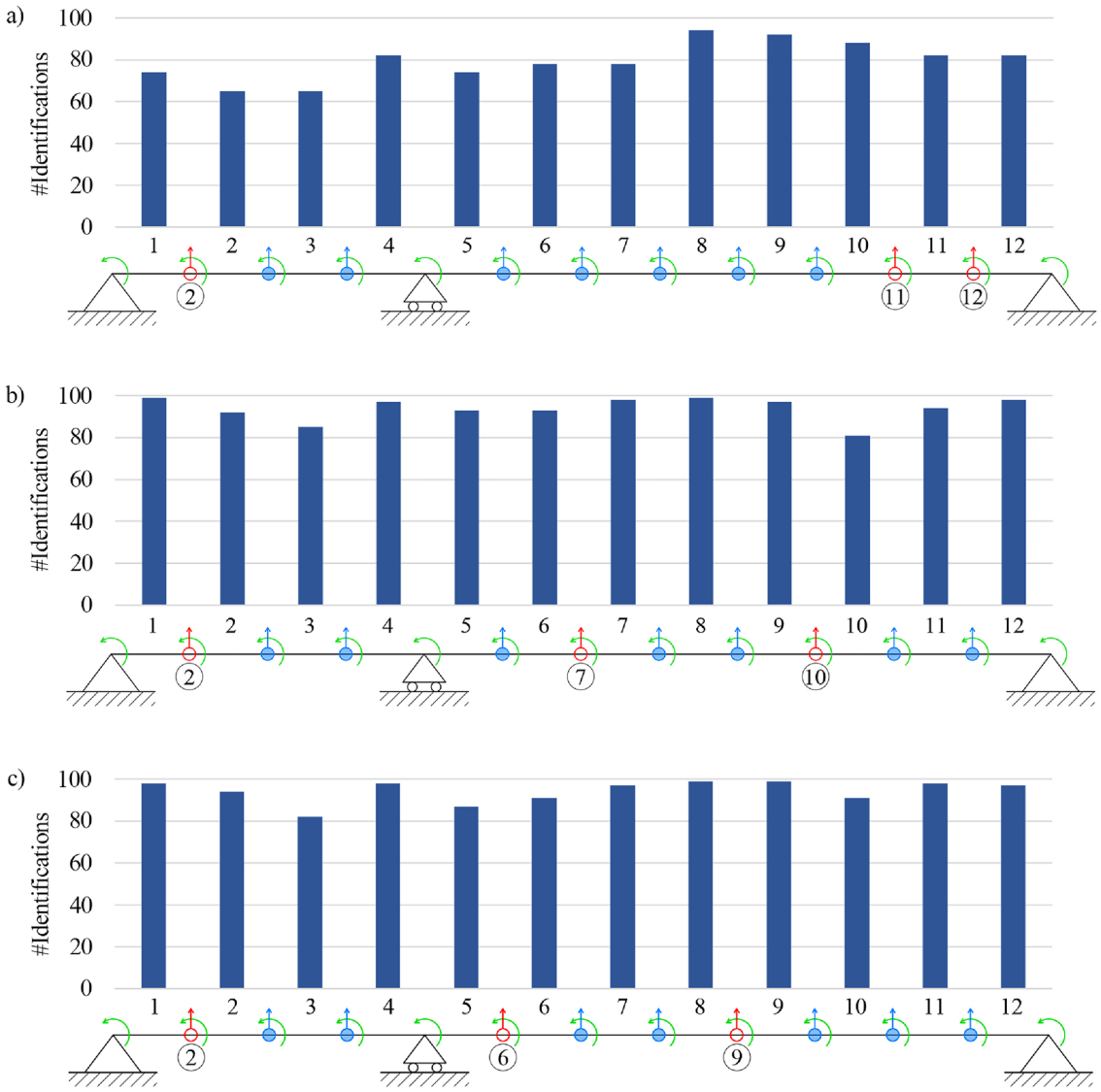

Fig. 7 Number of correct identifications over 100 runs in single damage scenarios (damage $d = 10\%$) with noise $p = 3\%$, considering **a** configuration C3, **b** configuration C4 and **c** configuration C6 for the control DOFs

This observation highlights two additional aspects that contribute to the robustness and reliability of the proposed method. First, for a fixed number of measured DOFs (i.e., considering the same set of sensors applied to the structure), identification results can be improved by considering different configurations of the degrees of freedom designated as control DOFs. This aspect will be investigated in the next section. Second, it is straightforward to check through numerical simulations which control points allow for increased accuracy in damage identification/localization, thereby informing in advance the deployment of the sensor network for the structure on-site. This highlights the applicability of the method to cases beyond the specific examples considered herein.

Let us now delve into the damage locations identified by the algorithm in cases of incorrect localizations. In other words, we aim to investigate whether the algorithm, when making incorrect identifications, localizes the damage in proximity to the real damaged element or gives random localization outputs.

The analyzed structure is the 12-element beam using the control sensor configuration C4. For the sake of brevity, only a damage scenario is presented, considering an elastic modulus reduction d equal to 10% and a noise level p equal to 3%.

Following a similar idea to the confusion matrix presented in [43], the matrix containing the identified locations of damage is shown in Fig. 9. Each column of the matrix is referred to as the real damaged element, while each row is related to the identified damaged element by the algorithm.

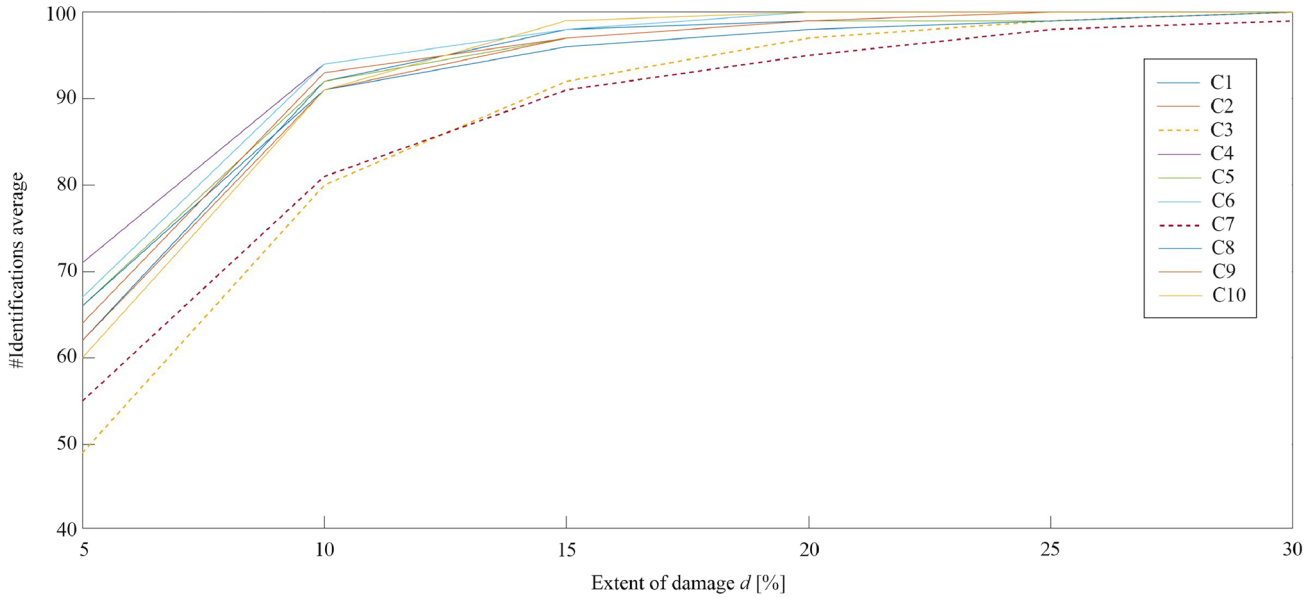

Fig. 8 Average number of correct identifications over 100 runs in single damage scenarios with different 3-control sensor configurations for increasing damage extent, noise $p = 3\%$

Therefore, the values along the diagonal represent the number of correct identifications, considered as the number of "true positives", while all values outside the diagonal pertain to incorrect localizations, i.e., "false positives".

Notably, for the elements with the lowest successful identification rate (i.e., elements 2, 3 and 10 in the matrix), the wrong identifications are located in the elements next to the real damaged one. For example, by simulating damage in element 10 (i.e., considering the 10^{th} column of the matrix), in 81 over 100 simulations the damage is correctly localized, while in the remaining 19 the elements 9 and 11, next to the real damaged one, are identified.

Identified element \ *Damaged element*	1	2	3	4	5	6	7	8	9	10	11	12
1	99	0	0	0	0	0	0	0	0	0	0	0
2	0	92	12	0	0	3	0	0	0	0	0	0
3	0	7	85	0	0	1	0	0	0	0	0	0
4	0	0	0	97	0	0	0	0	0	0	0	0
5	0	0	0	0	93	0	0	0	0	0	0	0
6	0	0	1	0	0	93	1	0	0	0	0	0
7	1	0	0	0	1	0	98	0	0	0	0	0
8	0	0	0	2	0	0	0	99	0	0	0	1
9	0	0	2	0	4	1	0	0	97	5	0	1
10	0	0	0	0	2	1	0	0	3	81	6	0
11	0	1	0	1	0	1	1	1	0	14	94	0
12	0	0	0	0	0	0	0	0	0	0	0	98

Fig. 9 Damage localization matrix, with damage $d = 10\%$, noise $p = 3\%$. Results obtained considering configuration C4 for the control DOFs

We can conclude that the algorithm, also in the case of wrong identifications, detects as damaged elements the ones close to the real one.

5.2 Double damage scenarios

In order to investigate the capability of the proposed algorithm to identify double damages, we consider two scenarios on the same beam: one involving damage in two non-adjacent elements (Fig. 10a), and the other scenario considering adjacent damaged elements (Fig. 10b). For the first configuration, elements 3 and 8 are damaged with a reduction in elastic modulus of 30% and 20%, respectively. For the second scenario, the damage is simulated in elements 5 and 6, with damage levels equal to 30% and 35%, respectively. The level of noise is set to $p = 3\%$.

In Fig. 10c) and Fig. 10d), results in terms of **CDI** index values versus the element number are reported. For both the scenarios, the index shows clear peaks in correspondence of the damaged elements. The identified values of the damage extent are equal to 15% of reduction in elastic modulus for both elements 3 and 8, while for adjacent elements 5 and 6, the procedure quantifies damage as 30% and 25%, respectively.

Indeed, the two-step algorithm correctly identifies locations of the damage, while it shows limitations in determining the severity of the damage. Both the extents of damage for elements 3 and 8 and the magnitude of damage for element 6 are underestimated. Nevertheless, for

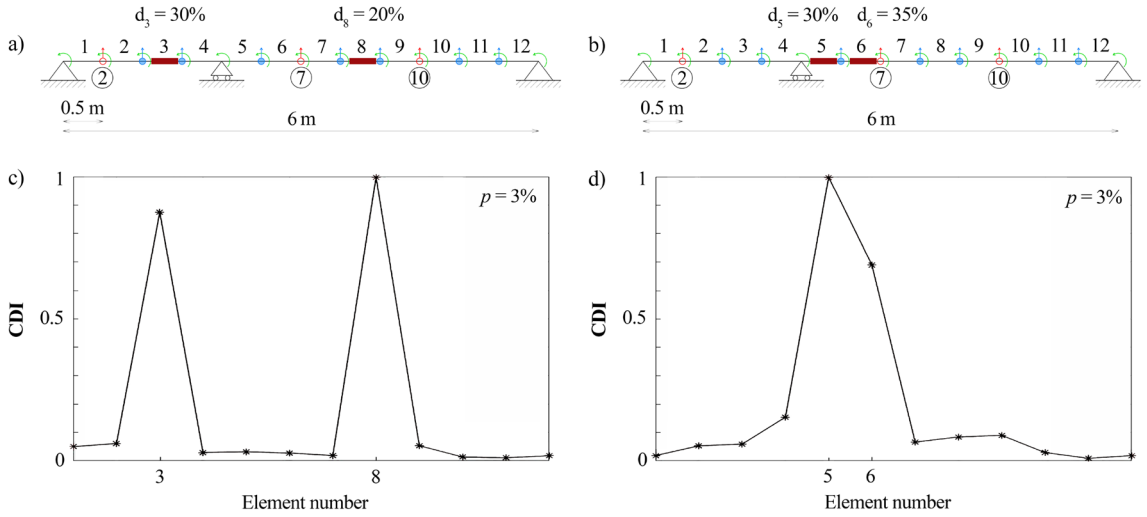

Fig. 10 Simulated double damage scenarios on the 12-element beam: **a** two non-adjacent and **b** two adjacent damaged elements. **CDI** index results: **c** for non-adjacent and **d** for adjacent damaged elements. Noise $p = 3\%$. **CDI** maximum normalized to 1

practical purposes in field applications, this level of accuracy may be sufficient.

6 Experimental validation

In this section, the proposed identification procedure is tested on two beam structures: a steel beam and a concrete beam. Specifically, the first beam was tested at the laboratory of University of Bologna considering three different damage scenarios, while experimental data on the concrete beam were collected at KU Leuven, [18, 19, 33, 34], and herein post-processed to identify extended damage scenarios.

6.1 Steel beam structure

The structure, tested at the LISG laboratory of the University of Bologna, is a simply-supported steel beam, characterized by a length of 2.4 m and a rectangular hollow cross-section, Fig. 11.

The chosen configuration for laboratory tests, in terms of discretization and boundary conditions, is shown in Fig. 12. The beam is divided into 30 equally spaced elements of 8 cm length.

A FE model of the beam considering the same discretization and the same constraints, is implemented. In particular, for the material properties, material density ρ is 7448 kg/m^3, while modulus of elasticity is set at 200 GPa to minimize the discrepancy between the numerical and experimental frequencies. Hinges at the boundary were considered appropriate to model the real supports.

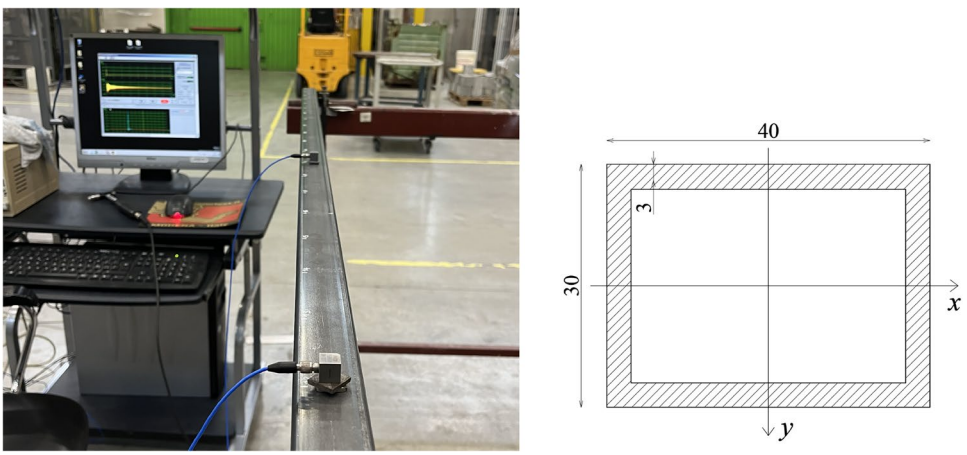

Fig. 11 On the left, experimental set-up of the simply supported steel beam under analysis and on the right, beam cross section. Dimensions in millimeters

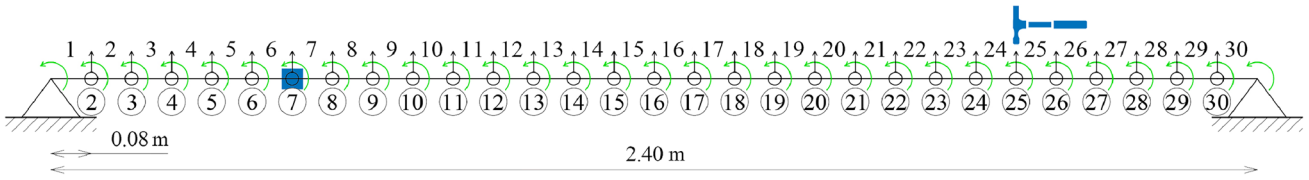

Fig. 12 Schematic of the steel beam: discretization, position of the fixed accelerometer (blue square) and of the hammer impact point

Dynamic tests are conducted through the so-called roving sensors approach, [44]. Two monoaxial piezoelectric accelerometers are used to record accelerations in the vertical direction. One sensor is fixed in place (and used as the reference accelerometer in the system identification process), while the other sensor position is changed to monitor all the other nodes of the beam. An instrumented hammer is used to excite the structure. To ensure that the modes of vibration are properly excited and identified, both the hammer impact point and the fixed accelerometer position are chosen to be as close as possible to the anti-nodes of the first four mode shapes. Nodes 7 and 25 are selected for the fixed sensor and the hammer impact, respectively, Fig. 12. Every point is excited at least three times, and the average of these measurements is considered in the calculations. The sampling frequency is set equal to $f_s = 1000$ Hz and 8192 points are recorded in every test. Following the described procedure, the steel beam in healthy conditions is tested.

Notably, all the vertical components of the mode shapes are measured ($k = 29$), while rotations are unknown ($u = 31$). Nevertheless, the proposed algorithm can be easily applied also when some vertical deflections are unknown. Here, the expansion of the known modal components is necessary also for the healthy structure to obtain the complete modal matrix $\mathbf{\Phi}^{\mathrm{H}}$, Eq. (26), to calculate the flexibility matrix for the intact beam $\mathbf{F}^{\mathrm{H}}$, Eq. (10). As stated in Sect. 4, the expansion operator $\mathbf{R}^{\mathrm{H}}$, Eq. (27), is obtained considering the stiffness and the mass matrices derived by the FE model.

Dynamic identification of the steel beam is performed using MACEC software and the reference-based combined deterministic-stochastic subspace (CSI/ref) algorithm proposed by Reynders and De Roeck [45]. MACEC allows the evaluation of modal parameters, such as natural frequencies, damping ratios, mode shapes, and modal scaling factors [46]. In MACEC, a pre-processing step is performed by removing the offset from the signals. The stabilization diagram is constructed from state-space systems identified with CSI/ref and the stable poles are selected to determine the modal properties of the beam.

Mode shapes identified with the modal analysis are scaled to unit norm. Such mass normalization, needed to evaluate the flexibility matrix, is performed considering the mass matrix obtained with the FEM analysis, after the evaluation of the rotations using the expansion technique.

Table 2 Experimental and FEM natural frequencies of the steel beam in healthy conditions

i	$f^{\mathrm{H}}_{i,\mathrm{FEM}}$[Hz]	$f^{\mathrm{H}}_{i,exp}$[Hz]	Variation [%]
1	16.66	16.04	3.71
2	66.65	63.33	4.97
3	149.95	150.82	−0.58
4	266.58	259.40	2.69

Natural frequencies $f^{\mathrm{H}}_{i,exp}$ $(i = 1, ..., 4)$ are listed in Table 2. In the same table, natural frequencies evaluated using the FEM $f^{\mathrm{H}}_{i,\mathrm{FEM}}$, are also reported showing the agreement with the experimental results.

After testing the beam in healthy conditions, three damage scenarios are considered, namely SD1, SD2 and DD as represented in Fig. 13:

- SD1 indicates the single damage scenario concerning the realization of a notch in element 12. In particular, damage affects a portion of the bottom flange for a length of 10 mm, and part of the lateral webs, as represented in Fig. 13a);
- SD2 scenario involves an increase of damage in element 12. In particular, the dimensions of the existing notch are modified as shown in Fig. 13b);
- in DD scenario an additional element, in particular element 23, is damaged realizing a notch in the bottom flange and lateral webs as shown in Fig. 13c).

We emphasize that the damage implemented in the algorithm differs from the physical damage applied to the beam. In the algorithm, damage is represented as a reduction in the bending stiffness of an entire beam element, while the real damage is obtained by reducing the cross-section for a specific length of the beam which differs from the discretization length. These discrepancies should be considered when interpreting the results of the algorithm. For this reason, quantification of damage is not carried out, as damage severity evaluated as an equivalent stiffness reduction is purely nominal.

The configuration, in terms of unknown, base, and control DOFs, used to detect, localize and quantify damage

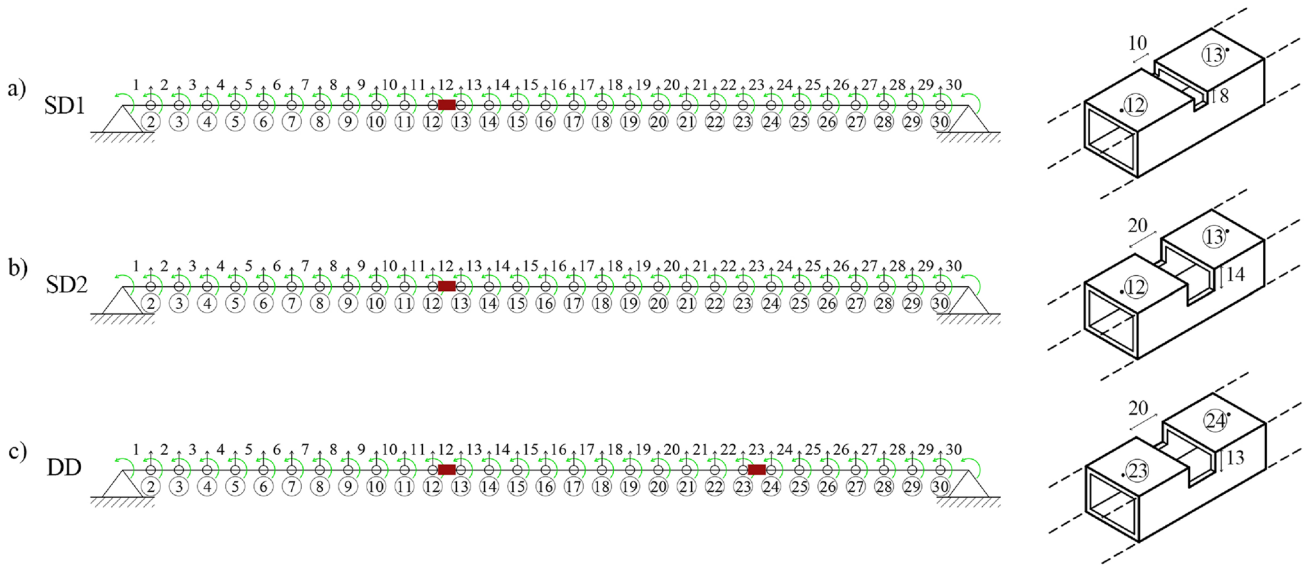

Fig. 13 Steel beam damage scenarios: **a** SD1 scenario, notch in element 12; **b** SD2 scenario, increased notch in element 12 and **c** DD scenario, additional notch in element 23. Dimensions in millimeters

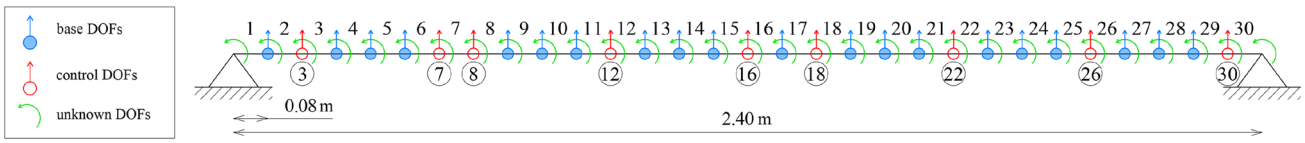

Fig. 14 Schematic of the beam: FE discretization (30 elements) and DOFs classification

in the steel beam is displayed in Fig. 14. In particular, the following parameters are adopted: the measured DOFs are $k = 29$, among which $c = 9$ DOFs are selected as control DOFs, while the remaining $b = 20$ are employed as base for the expansion procedure. All the rotations represent the unknown components ($u = 31$) to be evaluated using the expansion procedure.

6.1.1 Damage scenarios identification

The identification outputs for the damage scenario SD1 in terms of **CDI**, are presented in Fig. 15, showcasing the localization capabilities of the proposed approach. In particular, from **a** to **d**, the **CDI** vector is evaluated with an increasing number of mode shapes m used to calculate the flexibility matrix. In contrast with the results presented in the numerical tests of Sect. 5, we can observe that, as the number of mode shapes increases (especially after the second mode), the identification results become less accurate, even if element 12 is still identified as damaged. A possible reason is that mode shapes associated with higher natural frequencies are affected by a higher level of noise compared to the lower ones, thus impacting the accuracy of the method.

The identification results concerning the single damage scenario SD2 in terms of **CDI** values are presented in Fig. 16. It can be observed that the results are less noisy compared to the previous scenario, Fig. 15, as the values of **CDI** for the healthy elements of the beam are close to zero. This is attributed to the increasing capability of the algorithm to identify damage as the severity of damage extent increases. However, it is still noticeable that employing an increasing number of mode shapes m does not improve results due to the higher level of noise associated with higher modes. These results suggest the opportunity of using a reduced number of mode shapes for the identification of a single damage.

To further evidence the capabilities of the method in addressing damage localization with a reduced number of sensors, we replicate the damage localization for the experimental steel beam in the damage case SD2. Here, identification results are performed considering not only the rotations but also the vertical displacements at the nodes 4, 5, 10, 15, 17, 20, 25 and 29 as unknown, while keeping the same control DOFs. As can be seen in Fig. 17, the damage is correctly localized by the **CDI** and the outputs are comparable to those in Fig. 16, where all vertical modal components are known.

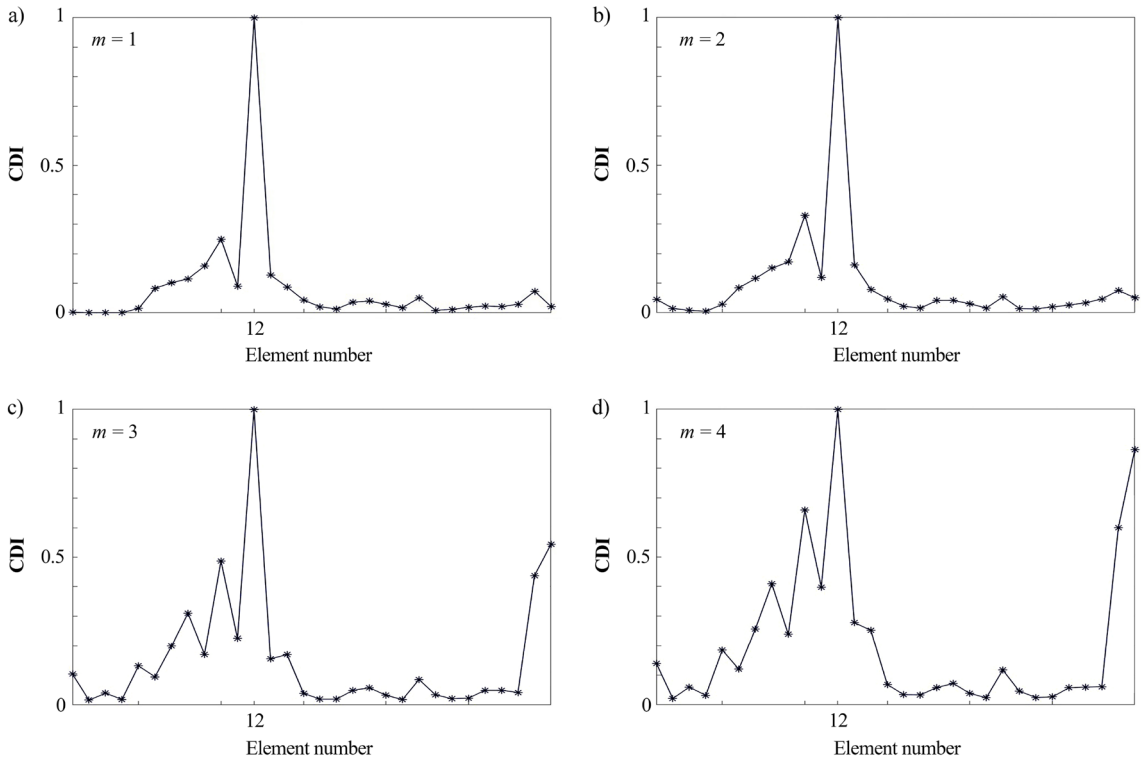

Fig. 15 SD1 damage scenario for the steel beam: **CDI** index considering **a** $m = 1$ mode, **b** $m = 2$ modes, **c** $m = 3$ modes and d) $m = 4$ modes. **CDI** maximum normalized to 1

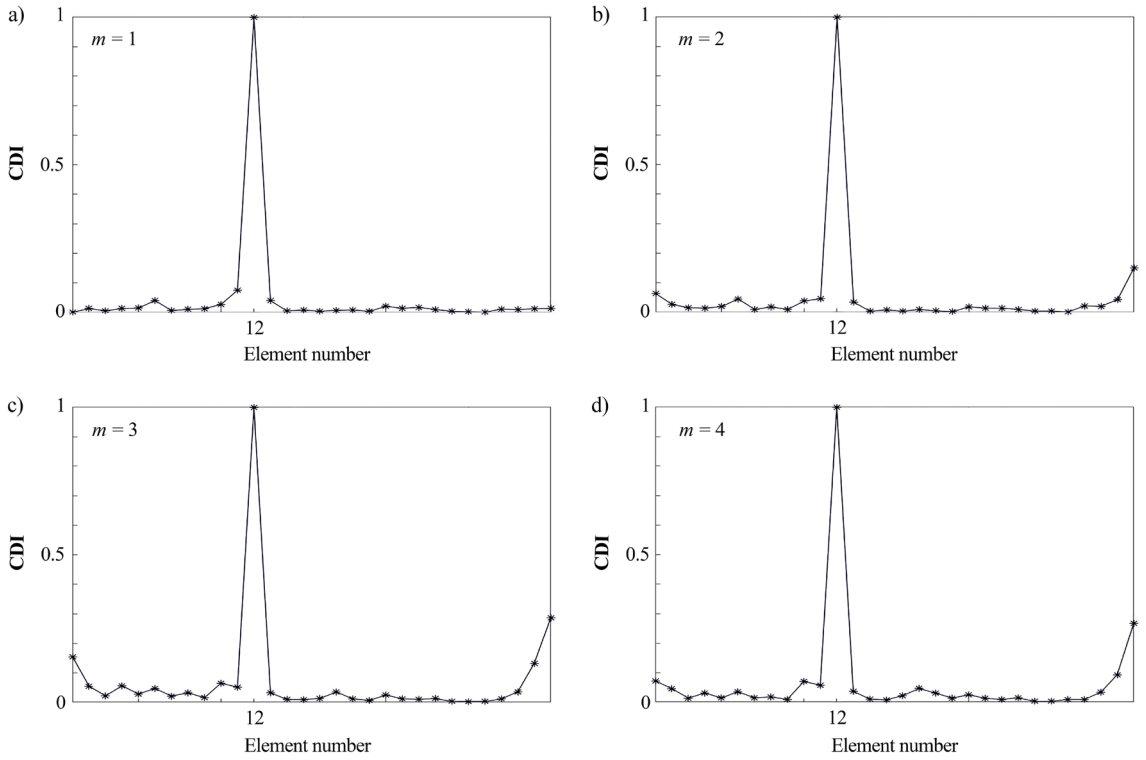

Fig. 16 SD2 damage scenario for the steel beam: **CDI** index considering **a** $m = 1$ mode, **b** $m = 2$ modes, **c** $m = 3$ modes and **d** $m = 4$ modes. **CDI** maximum normalized to 1

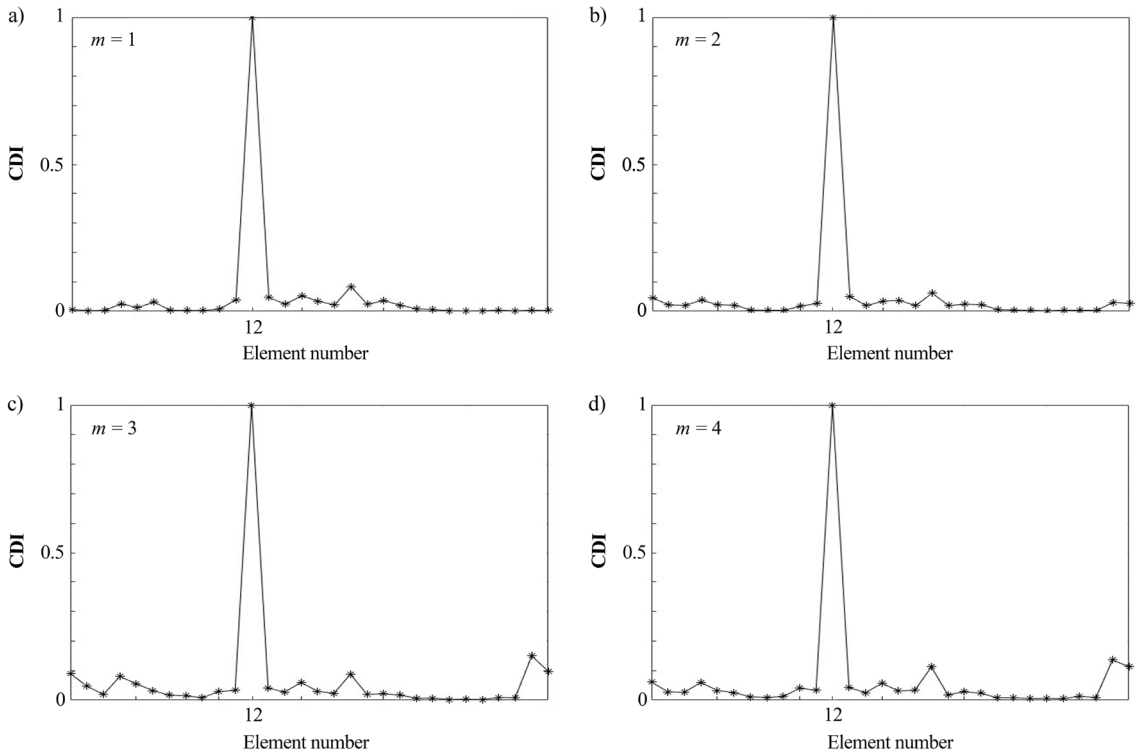

Fig. 17 SD2 damage scenario for the steel beam: **CDI** index considering a reduced number of measured vertical displacements and **a** $m = 1$ mode, **b** $m = 2$ modes, **c** $m = 3$ modes and d) $m = 4$ modes. **CDI** maximum normalized to 1

We now consider the DD scenario in Fig. 13c. Differently from what was observed in the single damage scenarios, a single mode shape is not sufficient to accurately locate both damages. With $m = 1$, as shown in Fig. 18a, the algorithm identifies elements 12 and 19 as the most likely damaged elements, while element 23 exhibits a lower peak than the other two. To address this issue, an increasing number of mode shapes is used to calculate the flexibility matrix. This leads to an accurate localization of the damaged elements, as shown in Fig. 18b, c, d for $m = 2$, $m = 3$, and $m = 4$, respectively.

Alternatively, in cases where additional modes cannot be acquired through experimental measurements, an improvement of identification outputs for $m = 1$ can be simply achieved adopting a coarser discretization of the beam and varying the position of the control DOFs, while maintaining the same set of measured components. To this aim, the beam is divided into 15 elements instead of 30. Notably, the damages are within the 6th and the 12th element in the 15-element discretization. The measured DOFs are $k = 14$ (all the vertical displacements), while the rotations are computed using the expansion procedure (unknown DOFs $u = 16$). Outcomes varying the number and position of the control DOFs are listed in Table 3. Specifically, out of the 14 measured DOFs, control DOFs $c = 4$ and $c = 5$ are selected. The results clearly show that element 6 is identified seven times, while element 12 is identified four times. Notably, elements 7 and 11 emerge in the other identifications, which are close to the actual damaged elements. Moreover, it is noteworthy that with this coarser mesh, the damages do not entirely involve the elements, and they are not precisely centered within elements 6 and 12, but rather positioned toward elements 7 and 11, respectively. Element 1 appears as an outlier in the identifications. Comparing these identification results with those represented in Fig. 18a, it can be correctly inferred that the most likely damaged elements are 12 and 23 in the fine mesh, which correspond to sub-elements of elements 6 and 12 in the coarser mesh.

Table 3 DD damage scenario for the steel beam: identified elements varying the control DOFs selection

Control DOFs	c	Identified elements
4, 8, 9, 12	4	7, 6
5, 8, 10, 13	4	12, 6
4, 7, 10, 13	4	11, 6
6, 7, 12, 13	4	12, 6
4, 6, 8, 11, 12	5	12, 6
5, 6, 8, 10, 13	5	12, 7
4, 7, 10, 12, 13	5	6, 11
6, 7, 9, 12, 13	5	1, 6

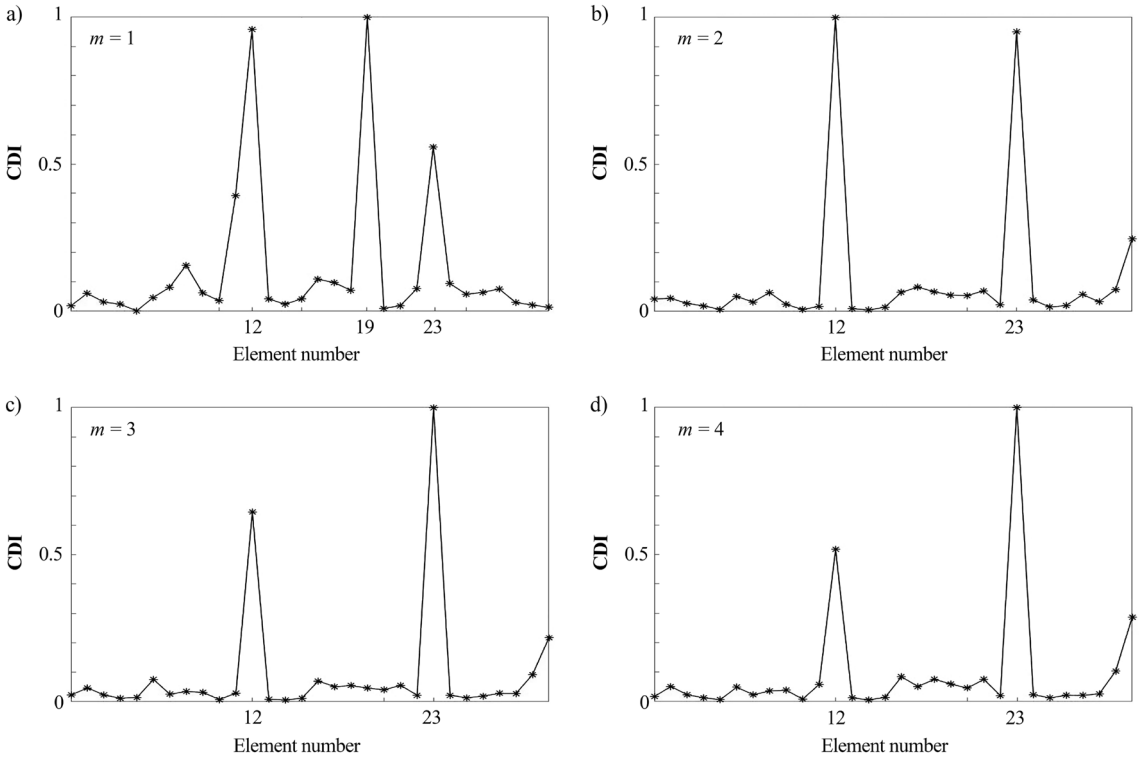

Fig. 18 DD damage scenario for the steel beam: **CDI** index considering **a** $m = 1$ mode, **b** $m = 2$ modes, **c** $m = 3$ modes and d) $m = 4$ modes. **CDI** maximum normalized to 1

Fig. 19 First damage scenario in the concrete beam corresponding to an applied load equal to 25 kN (step 5 in [34])

6.2 Concrete beam structure

The structure under investigation is a reinforced concrete beam, characterized by a length of 6.0 m, a $250 \times 200\,\text{mm}^2$ rectangular cross-section, density ρ equal to $2500\,\text{kg/m}^3$ and bending stiffness EI equal to $7.24 \times 10^6\,\text{Nm}^2$. A finite element model is developed based on the information provided in [33]. In particular, the beam is discretized in 15 beam elements. Free-free boundary conditions are considered to replicate the dynamics testing scenarios, as described in the following. The beam was tested for 12 increasing load steps at KU Leuven and the experimental campaign is described in [18, 19, 33, 34].

Details of the conducted tests on the beam are herein only briefly outlined. The beam was damaged using static three-point bending tests applying increasing levels of load. At each load increment, the beam was dynamically tested in free-free conditions, with the beam suspended with flexible springs, to obtain the modal characteristics. Modal identification of the concrete beam is carried out by processing the output data from KU Leuven using MACEC software and the reference-based combined deterministic-stochastic subspace algorithm, [45].

Table 4 Experimental natural frequencies of the concrete beam in healthy and damaged conditions

i	$f^{\text{H}}_{i,exp}$ [Hz]	$f^{\text{D}}_{i,exp}$ [Hz]	Decrease [%]
1	22.77	19.38	14.91
2	65.71	57.02	13.23
3	127.37	111.95	12.11
4	208.68	185.42	11.15

For brevity, in this work we analyze the beam in two damage scenarios. The first scenario, illustrated in Fig. 19, corresponds to a load of $P = 25$ kN. As depicted, the damage affects elements numbered from 8 to 13, as per the finite element discretization shown in Fig. 20. Natural

frequencies of the healthy $f^{H}_{i,exp}$, and damaged beam $f^{D}_{i,exp}$ ($i = 1, ..., 4$), are listed in Table 4.

By employing the DOFs discretization displayed in Fig. 20, the **CDI** outputs represented in Fig. 21 are obtained for increasing numbers of mode shapes. For increasing values of m, the identification improves progressively. It is noted, in particular, that using $m = 3$ mode shapes, the only values greater than zero are found precisely between elements 8 and 13, which are the damaged elements in the beam.

The second damage scenario under investigation is represented in Fig. 22, corresponding to a load $P = 19$ kN. Elements from 4 to 13 are characterized by cracks. The same discretization and configuration in terms of base, control and unknown DOFs as the ones adopted in the previous scenario are considered, Fig. 20.

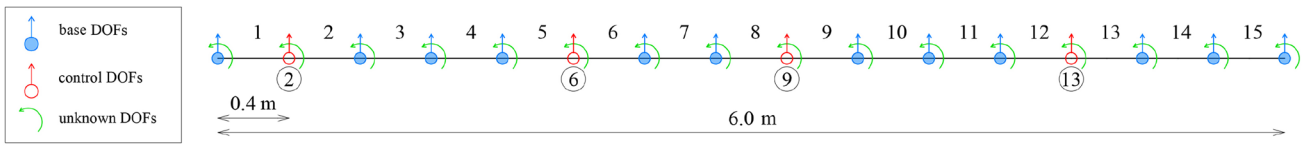

Fig. 20 Discretization and configuration, in terms of base, control and unknown DOFs, adopted for the **CDI** damage identification in the concrete beam

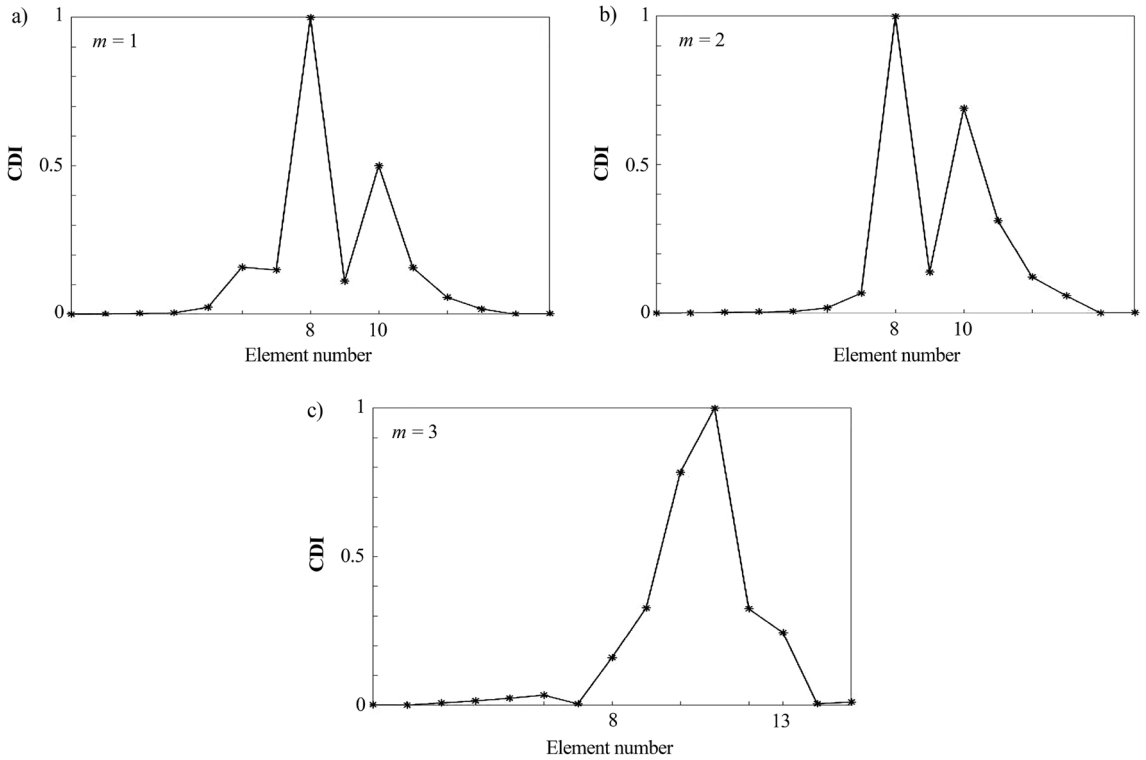

Fig. 21 First damage scenario for the concrete beam (step 5 in [34]): **CDI** index considering **a** $m = 1$ mode, **b** $m = 2$ modes and **c** $m = 3$ modes. **CDI** maximum normalized to 1

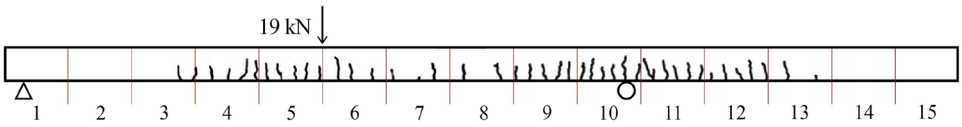

Fig. 22 Second damage scenario for the concrete beam corresponding to an applied load equal to 19 kN (step 9 in [34])

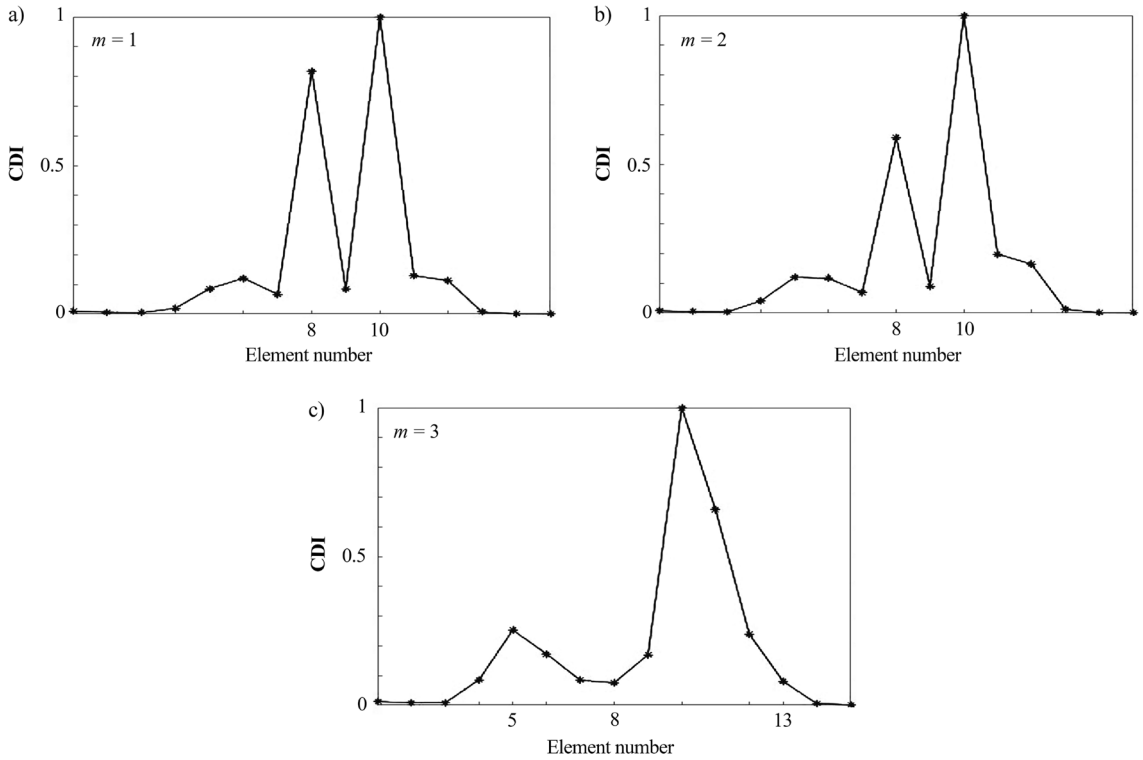

Fig. 23 Second damage scenario for the concrete beam (step 9 in [34]): **CDI** index considering **a** $m = 1$ mode, **b** $m = 2$ modes and **c** $m = 3$ modes. **CDI** maximum normalized to 1

Results are shown in Fig. 23, where the extensive damage scenario is correctly identified considering $m = 3$ mode shapes.

7 Conclusions

In this work, we presented a procedure based on a two-step algorithm for damage detection, localization and quantification in beam structures. The flexibility matrix was used to evaluate the Curvature Damage Index (**CDI**), based on the change in beam curvature between the healthy and the damaged structure. Due to the rapid convergence of the flexibility matrix for increasing values of natural frequencies and modes, curvature changes are accurately estimated considering only the lowest m natural frequencies and mode shapes of the structure.

The approach requires all the components of the selected first m mode shapes to be known. As in real applications only a limited number of components is available, we introduced an iterative procedure for the dynamic expansion of the measured components. The use of a limited number of measured components, namely the control components, in the expansion procedure provided a first estimation of damaged element and severity through the TMAC evaluation. In the following step of the procedure, this hypothesis was verified by computing the curvature damage index. Applying the procedure recursively, multiple damage scenarios were identified.

Numerical simulations and experimental tests were conducted on beam structures to check the accuracy of the proposed method. In the numerical tests, the algorithm was proved to be capable of detecting both single and double damages even of small severity (10% reduction of elastic modulus) despite the presence of noise. Results were shown to be slightly sensitive on the choice of control DOFs, provided that DOFs close to each other and simultaneously near the supports of the beam were not selected. The optimal ratio of control components to the overall number of known mode shape components is currently under investigation. Additionally, it was observed that when the damage position was not accurately determined, false positive identifications mostly corresponded to cases where the damage was located not in, but close to the actual damaged elements, thereby avoiding random outputs. This is a positive feature of the algorithm, as it ensures that potential control actions by operators are directed toward elements near the real damage. Notably, to improve identification results, we can either increase the number of modes used in calculating the flexibility matrix or change the position and number of control DOFs while maintaining the same set of measured components. The latter procedure is easy and fast to implement, as it requires

no additional field acquisitions, and it enhances the robustness of the algorithm, mitigating also the effect of noise. Moreover, using a coarser mesh of elements can help to limit uncertainties in identifications. A coarse discretization allows for the detection of damaged elements characterized by a low severity of damage, albeit with less precision in determining the exact damage location.

The proposed approach demonstrated good capabilities in assessing damage severity, although there was a slight underestimation in the double damage scenario. Notably, in real-world scenarios, defining damage as an equivalent stiffness reduction is purely nominal, as damage can manifest in various forms (corrosion, prestress loss, cracks, etc.). With these premises, our aim was not to quantify the exact extent of damage, but rather to identify an equivalent loss of stiffness, which can increase over periodic monitoring, replicating the progression of damage.

The experimental tests on a steel beam and a reinforced concrete beam showed the capability of the proposed procedure in identifying single, double and spatially extended damages. The influence of the number m of mode shapes used to evaluate the flexibility matrix on the identification results was studied.

Finally, we anticipate a few challenges that need to be addressed to apply the procedure to real-scale structures: (*i*) implementing a calibrated numerical model that accurately represents the real structure, (*ii*) properly accounting for the variability of dynamic properties due to environmental conditions, and (*iii*) establishing thresholds in the identification results to prevent false alarms for non-harmful situations. The initial attempts with lab-scale beams (both steel and concrete) yielded promising results in overcoming these challenges.

Overall, the methodology's robustness and ease of implementation make it suitable for supporting structural health monitoring strategies and damage identification tools for beam-like infrastructure such as bridges or viaducts.

Funding Open access funding provided by Alma Mater Studiorum - Università di Bologna within the CRUI-CARE Agreement.

Data Availability Data used in the numerical and experimental tests are available upon request.

Declarations

Compliance with Ethical Standards The authors declare that they have no conflict of interest.

References

1. Limongelli M, Celebi M (2019) Seismic Structural Health Monitoring - From Theory to Successful Applications. Springer, https://doi.org/10.1007/978-3-030-13976-6
2. Domaneschi M, Pellecchia C, De Iuliis E, Cimellaro GP, Morgese M, Khalil AA, Ansari F (2020) Collapse analysis of the polcevera viaduct by the applied element method. Eng Struct 214:110659. https://doi.org/10.1016/j.engstruct.2020.110659
3. Scattarreggia N, Salomone R, Moratti M, Malomo D, Pinho R, Calvi GM (2022) Collapse analysis of the multi-span reinforced concrete arch bridge of Caprigliola, Italy. Eng Struct 251:113375. https://doi.org/10.1016/j.engstruct.2021.113375
4. Modesti M, Palermo A, Gentilini C (2023) Finding damage in truss structures exploiting modal strains. In: Theoretical and Applied Mechanics: Aimeta 2022 (Materials Research Proceedings), pp. 145–150. https://doi.org/10.21741/9781644902431-24
5. Modesti M, Gentilini C, Palermo A, Reynders E (2023) Lombaert, G (2023) Identification of damage in truss and beam structures based on flexibility matrix. Exp Vib Anal Civ Eng Struct EVACES 2:632–640. https://doi.org/10.1007/978-3-031-39117-0_64
6. Modesti M, Reynders E, Lombaert G, Palermo A, Gentilini C (2024) Damage detection in beam structures based on curvature change estimated from incomplete mode shapes. J Phys 2647(18):182019. https://doi.org/10.1088/1742-6596/2647/18/182019
7. Alvandi A, Cremona C (2006) Assessment of vibration-based damage identification techniques. J Sound Vib 292(1):179–202. https://doi.org/10.1016/j.jsv.2005.07.036
8. Doebling SW, Farrar C, Prime MB (1998) A summary review of vibration-based damage identification methods. Shock Vibration Digest 30:91–105
9. Avci O, Abdeljaber O, Kiranyaz S, Hussein M, Gabbouj M, Inman DJ (2021) A review of vibration-based damage detection in civil structures: from traditional methods to machine learning and deep learning applications. Mech Syst Signal Process 147:107077. https://doi.org/10.1016/j.ymssp.2020.107077
10. Dilena M, Morassi A (2011) Dynamic testing of a damaged bridge. Mech Syst Signal Processi 25(5):1485–1507. https://doi.org/10.1016/j.ymssp.2010.12.017
11. Abdel Wahab MM, De Roeck G (1999) Damage detection in bridges using modal curvatures: Application to a real damage scenario. J Sound Vib 226(2):217–235. https://doi.org/10.1006/jsvi.1999.2295
12. Datteo A, Busca G, Quattromani G, Cigada A (2018) On the use of AR models for SHM: a global sensitivity and uncertainty analysis framework. Reliab Eng Syst Saf 170:99–115. https://doi.org/10.1016/j.ress.2017.10.017
13. Liu K, Law SS, Xia Y, Zhu XQ (2014) Singular spectrum analysis for enhancing the sensitivity in structural damage detection. J Sound Vib 333(2):392–417. https://doi.org/10.1016/j.jsv.2013.09.027
14. Janeliukstis R, Rucevskis S, Wesolowski M, Chate A (2017) Experimental structural damage localization in beam structure using spatial continuous wavelet transform and mode shape

curvature methods. Measurement 102:253–270. https://doi.org/10.1016/j.measurement.2017.02.005
15. Katunin A (2020) Damage identification and quantification in beams using Wigner-Ville distribution. Sensors 20(22):6638. https://doi.org/10.3390/s20226638
16. Chen H-P, Ni Y-Q (2018) Structural Health Monitoring of Large Civil Engineering Structures, pp. 155–193. John Wiley & Sons, Ltd, ???. Chap. 7 - Vibration-Based Damage Identification Methods
17. Pandey AK, Biswas M, Samman MM (1991) Damage detection from changes in curvature mode shapes. J Sound Vib 145(2):321–332. https://doi.org/10.1016/0022-460X(91)90595-B
18. Maeck J, De Roeck G (1999) Dynamic bending and torsion stiffness derivation from modal curvatures and torsion rates. J Sound Vib 225(1):153–170. https://doi.org/10.1006/jsvi.1999.2228
19. Maeck J, Abdel Wahab M, Peeters B, De Roeck G, De Visscher J, De Wilde WP, Ndambi J-M, Vantomme J (2000) Damage identification in reinforced concrete structures by dynamic stiffness determination. Eng Struct 22(10):1339–1349. https://doi.org/10.1016/S0141-0296(99)00074-7
20. Abdel Wahab MM (2001) Effect of modal curvatures on damage detection using model updating. Mech Syst Signal Process 15(2):439–445. https://doi.org/10.1006/mssp.2000.1340
21. Ciambella J, Pau A, Vestroni F (2019) Modal curvature-based damage localization in weakly damaged continuous beams. Mech Syst Signal Process 121:171–182. https://doi.org/10.1016/j.ymssp.2018.11.012
22. Zhang Y, Lie ST, Xiang Z (2013) Damage detection method based on operating deflection shape curvature extracted from dynamic response of a passing vehicle. Mech Syst Signal Process 35(1):238–254. https://doi.org/10.1016/j.ymssp.2012.10.002
23. Zhou Z, Wegner L, Sparling B (2007) Vibration-based detection of small-scale damage on a bridge deck. J Struct Eng 133:1257–1267. https://doi.org/10.1061/(ASCE)0733-9445(2007)133:9(1257)
24. Sampaio RPC, Maia NMM, Silva JMM (1999) Damage detection using the frequency-response-function curvature method. J Sound Vib 226(5):1029–1042. https://doi.org/10.1006/jsvi.1999.2340
25. Reynders E, De Roeck G, Bakir PG, Sauvage C (2007) Damage identification on the Tilff bridge by vibration monitoring using optical fiber strain sensors. J Eng Mech 2:185–193. https://doi.org/10.1061/(ASCE)0733-9399(2007)133:2(185)
26. Anastasopoulos D, De Roeck G, Reynders EPB (2019) Influence of damage versus temperature on modal strains and neutral axis positions of beam-like structures. Mech Syst Signal Process 134:106311. https://doi.org/10.1016/j.ymssp.2019.106311
27. Capecchi D, Ciambella J, Pau A, Vestroni F (2016) Damage identification in a parabolic arch by means of natural frequencies, modal shapes and curvatures. Meccanica 51:2847–2859. https://doi.org/10.1007/s11012-016-0510-3
28. Quaranta G, Carboni B, Lacarbonara W (2016) Damage detection by modal curvatures: numerical issues. J Vib Control 22(7):1913–1927. https://doi.org/10.1177/1077546314545528
29. Friswell MI, Garvey SD, Penny JET (1995) Model reduction using dynamic and iterated IRS techniques. J Sound Vib 186(2):311–323. https://doi.org/10.1006/jsvi.1995.0451
30. Balmes E (2000) Review and evaluation of shape expansion methods. Proc Int Modal Anal Conf—IMAC 1:555–561
31. Ding B-D, Feng D-S, Lv H-L, Li X (2017) Damage detection in grid structures using limited modal test data. Math Prob Eng **2017**https://doi.org/10.1155/2017/1089645
32. Qu Z-Q, Fu Z-F (2000) An iterative method for dynamic condensation of structural matrices. Mech Syst Signal Process 14(4):667–678. https://doi.org/10.1006/mssp.1998.1302
33. Maeck J (2003) Damage assessment of civil engineering structures by vibration monitoring. Ph.D. Thesis, Department of Civil Engineering, KU Leuven, Belgium
34. Reynders E, De Roeck G (2010) A local flexibility method for vibration-based damage localization and quantification. J Sound Vib 329(12):2367–2383. https://doi.org/10.1016/j.jsv.2009.04.026
35. Gao Y, Spencer B (2002) Damage localization under ambient vibration using changes in flexibility. Earthq Eng Eng Vib 1:136–144. https://doi.org/10.1007/s11803-002-0017-x
36. Pandey AK, Biswas M (1994) Damage detection in structures using changes in flexibility. J Sound Vib 169(1):3–17. https://doi.org/10.1006/jsvi.1994.1002
37. Montazer M, Seyedpoor S (2014) A new flexibility based damage index for damage detection of truss structures. Shock Vib 2014:1–12. https://doi.org/10.1155/2014/460692
38. Wu X, Xia J, Zhu X (2019) Finding damage localizations of a planar truss using modal strain energy change. Adv Civ Eng 2019:3040682. https://doi.org/10.1155/2019/3040682
39. Tarpø M, Nabuco B, Georgakis C, Brincker R (2020) Expansion of experimental mode shape from operational modal analysis and virtual sensing for fatigue analysis using the modal expansion method. Int J Fatigue 130:105280. https://doi.org/10.1016/j.ijfatigue.2019.105280
40. Papadimitriou C, Lombaert G (2012) The effect of prediction error correlation on optimal sensor placement in structural dynamics. Mech Syst Signal Process 28:105–127. https://doi.org/10.1016/j.ymssp.2011.05.019
41. Dessena G, Ignatyev DI, Whidborne JF, Zanotti Fragonara L (2023) A Kriging approach to model updating for damage detection. Lecture Notes Civ Eng 254:245–255. https://doi.org/10.1007/978-3-031-07258-1_26
42. Alkayem NF, Cao M, Zhang Y, Bayat M, Su Z (2018) Structural damage detection using finite element model updating with evolutionary algorithms: a survey. Neural Comput Appl 30(2):389–411. https://doi.org/10.1007/s00521-017-3284-1
43. Tiwari A (2022) Supervised learning: From theory to applications. In: Pandey, R., Khatri, S., Singh, N., Verma, P. (eds.) Artificial Intelligence and Machine Learning for EDGE Computing, pp. 23–32. Academic Press, https://doi.org/10.1016/B978-0-12-824054-0.00026-5
44. Amara Chandra C, Samal PK (2021) Experimental determination of mode shapes of beams by roving impact test. Materials Today: Proceedings 46, 9159–9163 https://doi.org/10.1016/j.matpr.2020.01.119 . International Mechanical Engineering Congress 2019
45. Reynders E, Roeck GD (2008) Reference-based combined deterministic-stochastic subspace identification for experimental and operational modal analysis. Mech Syst Signal Process 22(3):617–637. https://doi.org/10.1016/j.ymssp.2007.09.004
46. Reynders E, Schevenels M, De Roeck G (2021) MACEC 3.4 - The Matlab toolbox for experimental and operational modal analysis - User's manual